Three-Dimensional Reconstruction of Thermal Volumetric Sources from Surface Temperature Fields Measured by Infrared Thermography

Christophe Pradère[a], Marie-Marthe Groz[b], Emmanuelle Abisset-Chavanne[a], Anissa Meziane[a], and Alain Sommier[a]

[a]Univ. Bordeaux, I2M, CNRS, UMR 5295, Arts et Métiers Paris Tech, Bordeaux INP, F-33400 Talence, France
[b]Epsilon-Alcen company, Esplanade des Arts et Métiers, F-33405 Talence CEDEX, France

ABSTRACT

Non-destructive testing (NDT) of materials and structures is a very important industrial issue in the fields of transport, aeronautics and space as well as in the medical domain. Active infrared thermography is an NDT method that consists in providing an external excitation to cause an elevation of the temperature field in the material, consequently allowing evaluation of the resulting temperature field at the surface. However, thermal exciters that are used (flash lamps, halogen, lasers) act only on the surface of the sample. On the other hand, several energy conversion systems can lead to the generation of volumetric sources; the phenomena of thermo-acoustics, thermo-induction, thermomechanics or thermochemistry can be cited. For instance, ultrasonic waves can generate volumetric heat sources if the material is viscoelastic or if there is a defect. The reconstruction of these sources is the initial process for the quantification of parameters responsible for the heating. Characterizing a heat source means reconstructing its geometry and the supplied power. Identification of volumetric heat sources from surface temperature fields is a mathematically ill-posed problem. The main cause of the issue is the diffusive nature of the temperature. In this work, 3D reconstruction of the volumetric heat sources from the resulting surface temperature field, measured by infrared thermography, is studied. An analysis of the physical problem enables specifying the limits of the reconstruction. In particular, a criterion on the achievable spatial resolution is defined, and a reconstruction limitation for in-depth sources is highlighted.

Keywords: inverse problem; tomography; infrared thermography; non-destructive testing; 3D reconstruction

1. INTRODUCTION

Active infrared thermography is a widely used method in non-destructive testing (NDT). The process involves exciting the environment studied with the help of an external energy supply, and then measuring the resulting temperature on the surface. However, one of the disadvantages of thermal NDT is that the excitation and the measurement are on the surface. Indeed, exciters today used in thermal NDT are usually flash lamps, halogens or lasers, which act only on the surface of the material, making access to information in the volume difficult. Several energy conversion systems can, however, lead to the appearance of volumetric sources in a material: phenomena of thermo-acoustics, thermo-induction, thermomechanics or thermochemistry can be citenumd. For example, an excitation by ultrasonic waves can lead to heat sources in a material if it is viscoelastic or if it contains a defect. Thus, to characterize this defect or the parameter responsible for the heating, the first step is to characterize the volumetric heat source from the surface temperature data provided by the IR camera. This is a mathematically ill-posed problem, mainly because of the diffusive characteristic of the heat transfer problem as well as the influence of noise. This subject has first been studied as a 2D problem, where the objective was to reconstruct the size and the shape of planar subsurface defects from the blurred temperature measured at the surface Ref. 1.

Further author information: (Send correspondence to C. Pradere)
C. Pradere: E-mail: christophe.pradere@u-bordeaux.fr, Telephone: +33665034326

Then, the study has been extended to 3D problems; several pioneering teams have proposed methods based on thermal and acoustic coupling Refs. 2–6 or by introducing the concept of virtual waves Refs. 7, 8. These methods of reconstruction that exist today enable reconstructing volume data (sources, initial conditions, etc.) from surface data (temperature fields). However, two main limitations emerge from this work: depth and measurement noise. Indeed, whatever the methods used, the deep sources are poorly determined; they are blurred and etched, and their intensities are under-estimated. Finally, measurement noise, unavoidable during experiments is a limiting factor and drawback for the inverse processing method. To overcome this drawback, regularization methods allow approaching the solution, but the choice of the regularization parameters is delicate. The temporal shape of excitation used (modulated, burst, pulse, etc.) does not seem to be a decisive factor for reconstruction: the methods do indeed lead to similar results. Each of these methods has its advantages and disadvantages: methods that use pulsed excitation are, among others, fast but very sensitive to noise, unlike modulated excitation methods that are less sensitive to noise but slower to implement. In this paper, it is proposed to reconstruct 3D heat sources using a method based on an impulse excitation (Dirac type). The impulse thermal response has the advantage of being completely determined analytically. The main objective is to explain, using a physical criterion, the reason for the depth limitation. Then, a reconstruction process based on Bayesian inference, a method largely used in other scientific domains, is proposed to decrease the noise influence in the inverse processing. Finally, results on a complete 3D shape generated by the Joule effect will be presented.

2. METHODOLOGY OF THE INVERSION

2.1 Direct Problem

From the global point of view, the goal of the proposed method is to be able to reconstruct 3D volumetric sources $Q(x, y, z)$, as illustrated Figure 1, from the measured temperature fields at the sample surface opaque to IR radiation. With this constraint, we will assume that any geometry or shape of sources can be approximated by a sum of variable intensity source points.

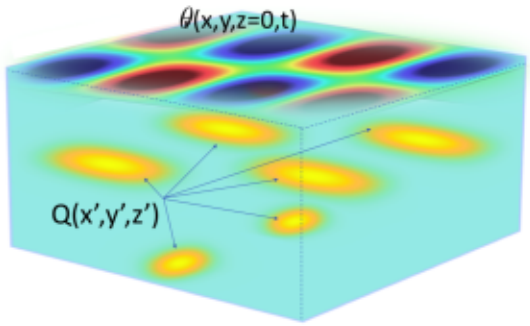

Figure 1. Schema of 3D volumetric sources distributed in a material and the associated surface temperature field.

The impulse thermal response θ_{Dirac} at each point $r = (x, y, z)$ at time t from a heat source located at $r' = (x', y', z')$ delivering, at a previous time t', a pulse of heat quantity of $Q(r')$ (J·m^{-3}) in an infinite homogeneous medium Ref. 9, possibly anisotropic, but of non-thermo-dependent thermophysical properties, is expressed analytically by Equation (1):

$$\theta_{\text{Dirac}} = \frac{Q(r')}{\rho C_p} G_{3D}\left(r, t/r', t'\right), \tag{1}$$

where ρ (kg·m^{-3}) and C_p (J·K^{-1}·kg^{-1}) are, respectively, density and specific heat of the material, while G_{3D} (m^{-3}) is the 3D-Green function of the material. This function can be written as:

$$G_{3D}\left(r, t/r', t'\right) = G_x\left(r, t/r', t'\right) \cdot G_y\left(r, t/r', t'\right) \cdot G_z\left(r, t/r', t'\right). \tag{2}$$

where G_x, G_y and G_z are the 1D-Green functions along the three directions of space Ref. 9.

If the domain is infinite in all three directions, each 1D-Green function expresses itself explicitly in the same way, here, with spatio-temporal Gaussian functions, and the thermal impulse response becomes:

$$\theta_{\text{Dirac}} = \frac{Q(x',y',z')}{\rho C_p} \frac{\exp\left(-\frac{(x-x')^2}{4a_x(t-t')}\right)}{\sqrt{4\pi a_x(t-t')}} \frac{\exp\left(-\frac{(y-y')^2}{4a_y(t-t')}\right)}{\sqrt{4\pi a_y(t-t')}} \frac{\exp\left(-\frac{(z-z')^2}{4a_z(t-t')}\right)}{\sqrt{4\pi a_z(t-t')}} \tag{3}$$

where a_x, a_y and a_z ($\mathrm{m^2{\cdot}s^{-1}}$) are the diffusivities along each of the x, y or z directions of space, respectively.

If the domain is not infinite in all three directions, but only along the directions x and y, and is only semi-infinite in the third direction (z), the 1D-Green functions Ref. 9 G_x and G_y are the same as in Equation (3), but G_z is different and can be written as:

$$G_z(z,t/z',t') = \frac{1}{4\sqrt{\pi a_z(t-t')}} \left[\exp\left(-\frac{(z-z')^2}{4a_z(t-t')}\right) + \exp\left(-\frac{(z+z')^2}{4a_z(t-t')}\right)\right]. \tag{4}$$

Now, if the domain is infinite along the directions x and y and finite along the direction z, the domain is therefore a plane sample of thickness L_z. In this case, the 1D-Green functions G_x and G_y are the same as in Equation (3), but G_z is different and can be written as Ref. 9 :

$$G_z(z,t/z',t') = \frac{1}{L_z}\left[1 + 2\sum_{m=1}^{+\infty} \exp\left(-a_z m^2\pi^2(t-t')/L_z^2\right)\cos\left(m\pi z/L_z\right)\cos\left(m\pi z'/L_z\right)\right]. \tag{5}$$

For this example of a sample finite along the z direction, the quadripole method is another technique that allows the access to the temperature response Ref. 10. It enables calculating the analytical solution $\overline{G_z}$ of G_z in the Laplace domain:

$$\overline{G_z}(z,p) = \frac{\cosh\left(z\sqrt{p/a}\right)\cosh\left((L-z')\sqrt{p/a}\right)}{\lambda\sqrt{p/a}\sinh\left(L\sqrt{p/a}\right)} \tag{6}$$

The previous Equation (6) can be inverted numerically to find its original in temporal space. The numerical algorithms, such as Gaver-Stehfest, or a return of Laplace by Fourier Ref. 10 or using De Hoog's Invlap algorithm, can indeed be used.

For the inversion, several models, including those defined by Equations (3), (4), (5) or (6), can be used. To compare the influence of each model along the z direction, three different configurations of heat sources are tested. As the x and y direction are considered infinite, the heat sources considered on the examples are an infinite plane along these dimensions, located at a given depth in the sample, as illustrated by Figure 2a.

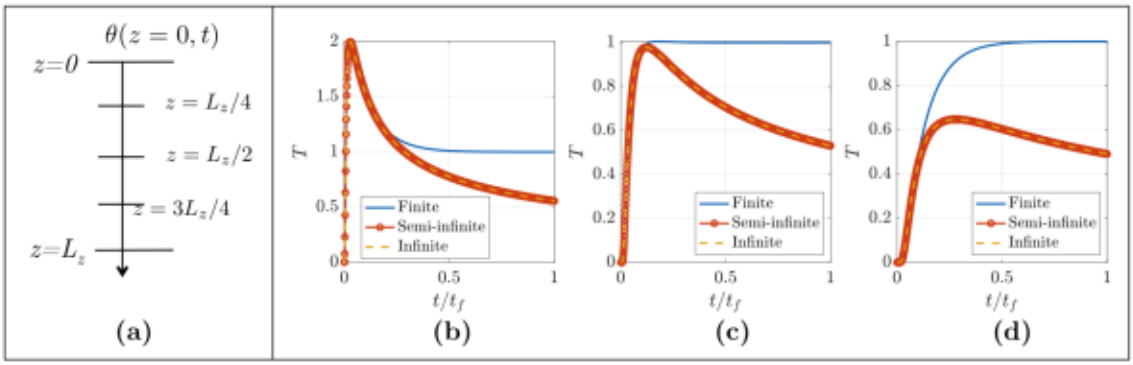

Figure 2. Scheme of the sample along the z direction (**a**). Temperature response at the surface depending on the used model for three configurations: a heat source located at $z = L_z/4$ (**b**), $z = L_z/2$ (**c**) or $z = 3L_z/4$ (**d**).

The first example is computed considering this heat source at $z = L_z/4$ (near the measuring surface). On the second example, the source is located at $z = L_z/2$ and for the last one, it is located at $z = 3L_z/4$ (deep source). The resulting temperatures $\theta(z = 0, t)$, are calculated by three different models (finite, semi-infinite and infinite along z), measured at the surface, and given by (b), (c) and (d), respectively, in Figure 2. For the three examples, $Q_0 = 0.01$ J·m^{-3}, $a = 2.5 \times 10^{-7}$ m^2·s^{-1} and $\rho C_p = 10^6$ J·K^{-1}·m^{-3}. The study is made between $t_0 = 0$ and $t_f = L_z^2/a$.

Whatever the depth of the heat sources, it can be seen that for short times, the temperature responses calculated by the three different models are exactly the same. The differences occur only for the long times.

In this paper, all the works were done at short times ($t < t_f/3$). Therefore, the model used is the infinite model, given by Equation (3), because it is more convenient (analytically). However, the choice of the model is not decisive: the methodology that leads to the results is the same, and any models or numerical simulations can be used for the inversion.

By introducing the following dimensionless data $t^* = \frac{t}{t_f}$, $i^* = \frac{i'}{L_i}$ ($i = x, y$ or z), as well as the Fourier number $Fo_i = \frac{a_i t_f}{L_i}$, where t_f corresponds to the time of the experiment and L_i to the considered length of the material, Equation (3) can be rewritten in dimensionless form as follows:

$$\theta_{3D}(x^*, y^*, z^*, t^*) = \frac{Q(x'^*, y'^*, z'^*)}{8\rho C_p L_x L_y L_z} \frac{\exp\left(\frac{(x^* - x'^*)^2}{4Fo_x t^*}\right)}{\sqrt{\pi Fo_x t^*}} \frac{\exp\left(\frac{(y^* - y'^*)^2}{4Fo_y t^*}\right)}{\sqrt{\pi Fo_y t^*}} \frac{\exp\left(\frac{(z^* - z'^*)^2}{4Fo_z t^*}\right)}{\sqrt{\pi Fo_z t^*}}. \tag{7}$$

Then for a given shape of a source the resulting temperature will be obtained by:

$$\theta(r^*, t^*) = \int_{\text{sample}} Q(r'^*)\theta_{3D}(r^* - r'^*, t^*)dr'. \tag{8}$$

In the case of the 3D problem, the whole material is discretized and each point of discretization is the representation of a voxel considered as a potential source, with a level of energy $Q(x_0, y_0, z_0) = Q_0\Omega(x_0, y_0, z_0)$, which corresponds to the mean of the source energy on the defined voxel. The size of the voxels depends on the number of discretizations along each direction. The problem is then written in matrix form, given by Equation (9). The resulting surface temperature at $z = 0$ is a 2D field as a function of time. For the writing of the problem, each $\theta(i)$ is a vector containing the 2D temperature reshaped into a 1D transient temperature:

$$\begin{pmatrix} \mathbf{I}_{3D}^{(1)} & \mathbf{I}_{3D}^{(2)} \cdots & \mathbf{I}_{3D}^{(n)} \end{pmatrix} [\Omega] = \begin{bmatrix} \theta_{(1)} \\ \theta_{(2)} \\ \vdots \\ \theta_{(m)} \end{bmatrix} \Leftrightarrow \mathbf{I}\ \Omega = \theta, \tag{9}$$

where $\mathbf{I}$ is an m by n operator matrix and θ is a vector of size m, and m and n are, respectively, the number of time steps and the depth discretization of the sample. n can then be seen as the number of point heat sources present in the material. In the case of the 3D problem, the operator matrix can indeed be written in the form of a block symmetric Toeplitz matrix Ref. 11:

$$\mathbf{I}_{3D} = \begin{pmatrix} A_1 & A_2 & \cdots & A_{n_x} \\ A_2 & A_1 & \ddots & A_{n_x-1} \\ \vdots & \ddots & \ddots & \vdots \\ A_{n_x} & A_{n_x-1} & \cdots & A_1 \end{pmatrix}, \tag{10}$$

where each element A_i is a matrix of size $n_t n_y$ by $n_z n_y$, n_z and n_y corresponding to the number of discretization points in z and y, and n_t to the number of time steps. All the matrices A_i are themselves symmetrical in blocks,

defined by:

$$A_i = \begin{pmatrix} A_{i1} & A_{i2} & \cdots & A_{in_y} \\ A_{i2} & A_{i1} & \ddots & A_{in_y-1} \\ \vdots & \ddots & \ddots & \vdots \\ A_{in_y} & \cdots & \cdots & A_{i1} \end{pmatrix}, \tag{11}$$

where each block A_{ij} is of size n_t by n_z. The global matrix $\mathbf{I}$ is therefore $n_x n_y n_t$ by $n_z n_y n_x$. Thus, instead of calculating all the points separately, just calculate the first row (by block) of each matrix A_i to reconstruct the entire matrix. The time savings by doing so are considerable. Indeed, for the 3D problem, the number of computations is $(n_x n_y)^2 n_z$.

3. DESCRIPTION OF SEVERAL INVERSE PROCESSING METHODS

In this part the main goal is to present the two main techniques developed by our team and to highlight their advantages and drawbacks.

3.1 Method based on Fourier criterium and regularization

The inverse problem given by Equation (9) is written as follows:

$$\mathbf{I}\,\Omega = \theta. \tag{12}$$

In practice, $\mathbf{I}$ is not square. Its number of lines is much greater than its number of columns. Therefore, $\mathbf{I}$ is not invertible. The algorithm used for the studied problem is therefore based on the Moore-Penrose pseudo-inversion method Refs. 12, 13. The pseudo-inverse $\mathbf{I}$ is obtained by using singular value decomposition (SVD) method Refs. 14–17. The principle of SVD is to decompose the matrix $\mathbf{I}$ of size m by n into a product of three matrices where $\mathbf{U}$ is an orthogonal matrix of size m by m, orthogonal $\mathbf{V}$ of size n by n and $\mathbf{S}$ a "diagonal" matrix of size m by n. The diagonal elements of $\mathbf{S}$ are called singular values. They are positive and ranked from the largest to the smallest.

If only the first p singular values are different from zero ($p < n$), the SVD can then be further reduced. Thus, the pseudo-inversion of Equation (18) gives:

$$\Omega = \sum_{k=1}^{p} \frac{\mathbf{U}_{\cdot,k}^T \theta}{s_k} \mathbf{V}_{\cdot,k}. \tag{13}$$

The reconstruction problem studied here responds well to the existence and uniqueness requirements of a well-posed inverse problem (cf. Hadamard Ref. 18). Unfortunately, the condition of stability is not respected. One of the methods to study this stability is to observe singular values of operator matrix $\mathbf{I}$: the closer they are to zero, the more the problem is ill-posed. If, in addition, their decay follows a power law such that if $s_i \approx i^{-n}$, with n strictly positive, the problem is described as ill-posed. On the other hand, if their decay follows an exponential law such as $s_i \approx e^{-i}$ (which is the case here), then it is strongly ill-posed. Then to overcome such problems, it becomes necessary to use regularization methods.

Mathematically, in the presence of noise, Equation (18) is no longer valid: strict equality becomes an approximation and inversion can be seen as a minimization problem by the least squares. The unknown Ω is sought in such a way as to minimize the residual R by the introduction of a term of penalization:

$$R^2 = \|\mathbf{I}\,\Omega - \theta_{mes}\|_2^2 + \alpha J(\Omega), \tag{14}$$

where α is a scalar called the "coefficient of regularization" and $J(\Omega)$ is an independent function of the unknown Ω. The higher the coefficient of regularization is, the more stable the inversion will be. However, in return, the term of "penalization" adds a bias to the initial problem. Thus, the greater the term of regularization is, the farther the final solution is from the good one. The difficulty therefore lies in the choice of the adjustment parameters in order to have the best compromise between stability and speed of the solution. Different methods

enable choosing the α parameter, among them the UPRE (unbiased predictive risk estimator), GCV (generalized cross validation), L-Curve and discrepancy principle or Picard methods Refs. 17, 19–23. Then, several types of regularization are possible depending on the choice of J. In this paper, the following types will be studied: (i), regularization by the L_2 standard (Tikhonov regularization Ref. 24), and (ii), regularization by the L_1 standard (Lasso method Ref. 25).

In the Tikhonov case, Equation (13) will take the following form:

$$\Omega = \sum_{k=1}^{p} \frac{s_k^2}{s_k^2 + \alpha} \frac{\mathbf{U}_{\cdot,k}^T \theta_{mes}}{s_k} \mathbf{V}_{\cdot,k}. \tag{15}$$

The comparison between the theoretical solution, given by Equation (13), and the solution of the Tikhonov regularization, given by Equation (15), shows that Tikhonov regularization has the effect of weighting each mode k of the SVD by a coefficient. In the L_1 regularization, Equation (13) will take the following form:

$$\left(\mathbf{V}\mathbf{S}^T\mathbf{S}\mathbf{V}^T + \alpha \left(\mathbf{J_{(i)}}\right)^2\right) \Omega_{(i)} = \mathbf{V}\mathbf{S}\mathbf{U}^T\theta_{mes}, \tag{16}$$

where for each iteration i, $\mathbf{J_{(i)}}$ is a diagonal matrix that contains the L_1-norm of the solution of the previous iteration $\Omega_{(i-1)}$. As can be seen in the definition of this matrix, each iteration uses the results from the source $\Omega_{(i)}$ from the previous iteration. For the first iteration, it is therefore necessary to define the matrix $\mathbf{J_{(1)}}$. The choice of this initialization does not matter, since from the first iteration, there will be correction according to the data of the inversion. However, it is unadvisable to take the null matrix since that would mean that the first iteration is not regularized. In this study, we take $\mathbf{J_{(1)}} = Id$, the identity matrix.

The problem given by Equation (16) is a simple linear equation, given by:

$$\mathbf{I_{L_1}}\, \Omega = \mathbf{V}\mathbf{S}\mathbf{U}^T\theta_{mes}. \tag{17}$$

The matrix $\mathbf{I_{L_1}}$ is entirely determined since it involves only the data of SVD of the matrix of the basic problem, as well as the solution $\Omega_{(i-1)}$ of the previous iteration (so known). Moreover, by its construction, this matrix is square and invertible. The resolution of the problem (17) can therefore be done via any inversion algorithm. Unlike Tikhonov's regularization and truncation of the spectrum of SVD, the regularization by the L_1-norm allows penalizing each position of the source (node of discretization) with a different parameter. As it is defined, regularization by the L_1-norm strongly penalizes the "zero" zones (no source), and conversely, it lowly weights non-zero areas (source). This approach favours a solution containing a maximum of null values, which results in strong intensity contrasts on the source reconstruction in contrast to the Tikhonov regularization, which tends to smooth the solution.

3.2 Method based on Bayesian inference

The inverse problem is still given by Equation (9) and again written as follows:

$$\mathbf{I}\,\Omega = \theta. \tag{18}$$

In the probabilistic framework, the idea is to reconstruct the repartition of the probability η of finding a source at each position i knowing the temperature evolution at the surface $\theta_{(j)}$, $j = 1...m$ using Bayesian inference based on the Bayes relations Ref. 26:

$$\eta(\Omega|\theta) = \frac{P(\theta|\Omega) \cdot P(\Omega)}{P(\theta)} \tag{19}$$

where $\eta(S|\theta)$ is called the posterior—the probability of source repartition S knowing the surface temperature θ—$P(\Omega)$ is the prior, $P(\theta|\Omega)$ is the likelihood—the probability of obtaining θ knowing S—and $P(\theta)$ is the model evidence.

In our case, the prior, which allows an *a priori* knowledge of η to be taken into account, is assumed to be irrelevant; the probability of finding a source is the same for all positions.

Therefore, in our case, the posterior can be written as follows Ref. 27:

$$P(\Omega|\theta) \propto \exp\left(-\frac{1}{2\Gamma^2}||\theta - \theta_{forward}(\Omega)||_2^2\right). \tag{20}$$

where $\theta_{forward}(\Omega)$ is the surface temperature evolution depending on the source repartition Ω.

To bypass the complexity of the problem when dealing with a 3D case due to the source position combinatorial explosion, it si proposed to treat the 2D temperature field as $n_x \times n_y$ independent 1D problems. Indeed, looking at the temperature only above the source allows us to limit the quantity of data to process without loosing much information as almost all the information is contained in it. Moreover, two other points are used to go on alleviating the combinatorial explosion: i) the superposition principle of the thermal response, coming from the linear characteristic of the problem, and ii) the fact that the sources are detected from the one closest to the surface to the deepest one, allowing for a sequential detection. Then, as soon as the position of a source is located $\Omega(S_1)$, its 3D analytical effect given by Equation (7) is subtracted from the measured temperature field θ_{mes} using equation (21):

$$\theta^\star(x, y, t) = \theta_{mes}(x, y, t) - \mathbf{A}_{3D}\Omega_{S_1}(x, y, t) \tag{21}$$

The source detection then goes on using the corrected surface temperature $\theta^\star(t)$ until the time interval has elapsed and all the sources have been detected.

Note that in the 3D case, the analytical contribution that is subtracted from the measured temperature field corresponds to 3D analytical solution given by eq (7). Thus the contribution of this source on the surface at any further timestep is eliminated.

4. RESULTS AND DISCUSSION

As depicted in Figure 3, the experiment in this part uses the Joule effect: a Chromel wire (nickel-chrome), traversed by a current transmitted by a generator, constitutes the heat source (a). The principle of the method is to insert this Chromel thread into PVC (polyvinyl chloride) material to form a particular geometrical figure. In this experiment, the diameter of the Chromel wire was 200 μm, and its geometric shape was similar to an "M", placed on the rear face of a PVC sample of 1 mm thickness. To avoid thermal losses on the side of the sample where the wire is located, a thickness of mousse has been bonded, thereby fixing the heating wire (b). The Chromel wire lies on a small area of the PVC sample, as illustrated in (c); therefore it can be considered semi-infinite along the x and y directions.

The Chromel wire is bonded to the back of the PVC sample. To estimate the whole 3D effect, the method of the images is used: the sample is then considered to be 2 mm thick with the wire located not on its backside but on the middle of the plane. Thus, at the time of reconstruction, one should find the Chromel wire centred on the middle plane of the sample along the z direction.

The PVC is supposed to be isotropic, with a density of $\rho = 1180\,\mathrm{kg{\cdot}m^{-3}}$, a heat capacity of $C_p = 1000\,\mathrm{J{\cdot}kg^{-1}{\cdot}K^{-1}}$, and diffusivity $a = 1.2 \times 10^{-7}\,\mathrm{m^2{\cdot}s^{-1}}$. The voltage of the generator was $U = 3.5\,\mathrm{V}$ with an intensity $I = 1.13\,\mathrm{A}$. The measures were carried out by an IR camera, with an acquisition frequency of 200 Hz, and the size of the pixel at the surface was 290 μm $\times$ 290 μm. In this experiment, the wire is traversed by the electric current for a duration of approximately 7 s. The area of study on which the temperature is measured as a function of time (with the IR camera) is a rectangle of dimensions $3.65 \times 2\,\mathrm{cm^2}$, divided into 126×72 pixels. The resulting field (*Digital Level*) at the surface is presented in Figure 4 at $t = 0\,\mathrm{s}$ when the power supply is turned on (a), after 2 s (b), after 7.2 s, where the maximum of the temperature is measured (c), and after 70 s (d).

Both methods, the one with Fourier criterium and the Bayesian one are applied to the previous experimental data and the retrieving 3D heat sources corresponding to the hot wire are represented in the figure 5 for the first method and in the figure 6 for the second one.

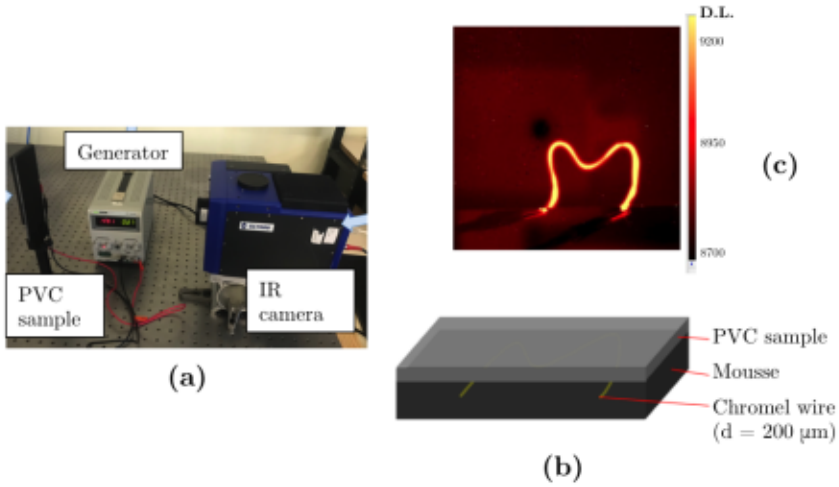

Figure 3. Picture of the experimental setup (**a**), schema of the home-made reference sample (**b**) and picture of the sample during the experiment (**c**).

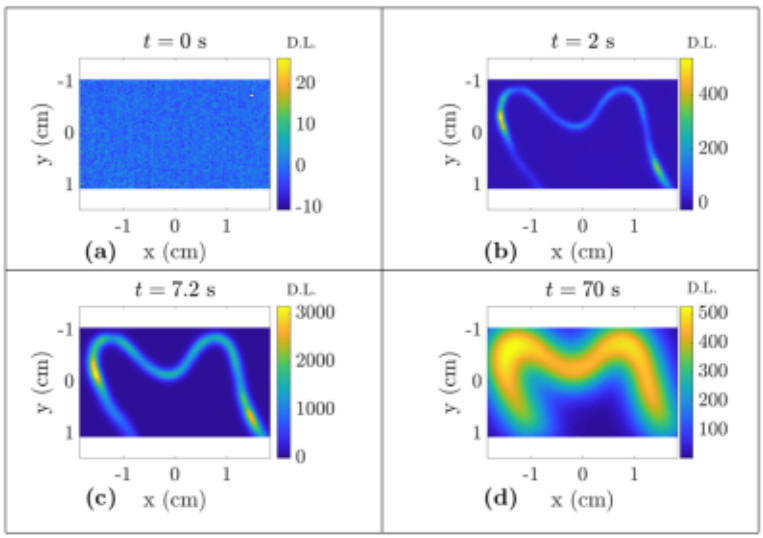

Figure 4. Measured temperature fields at the surface of the sample (PVC side): at $t = 0$ s when the power supply is turned on (**a**), after 2 s (**b**), after 7.2 s (**c**) and after 70 s (**d**).

Considering inversion with the first method (SVD + regularization), to avoid excessive computation time, the domain is divided into 18 equal parts (region of interest). Each of these domains is treated in a completely independent way. This division is possible because the heat sources are small (the ROI are semi-infinite comparing to the wire size) and the estimation are performed at short time, thus limiting the distribution in the plane. In each of the eighteen domains, the solution computed by the program is a cube (3D matrix) of values close to zero at points that do not contain sources and high values (which correspond to the intensity of the source) whenever there is a heat source. The juxtaposition of all the domains enables estimating the totality of the studied volume. For this experiment, the inversion with a regularization L_1 was computed on a dual processor with RAM = 128 GB: the duration of the algorithm was 5 h 45 min. Figure 5 illustrates the obtained results: view along the thickness (a) and along the x and y plane (b).

For the second method (Bayesian), it is assumed that the intensities of the thermal sources generated by the wire are identical and constant in all points. Under this hypothesis, the problem can be written in such a way as to search only for the position of the thermal sources (and not their intensities). After a normalisation of

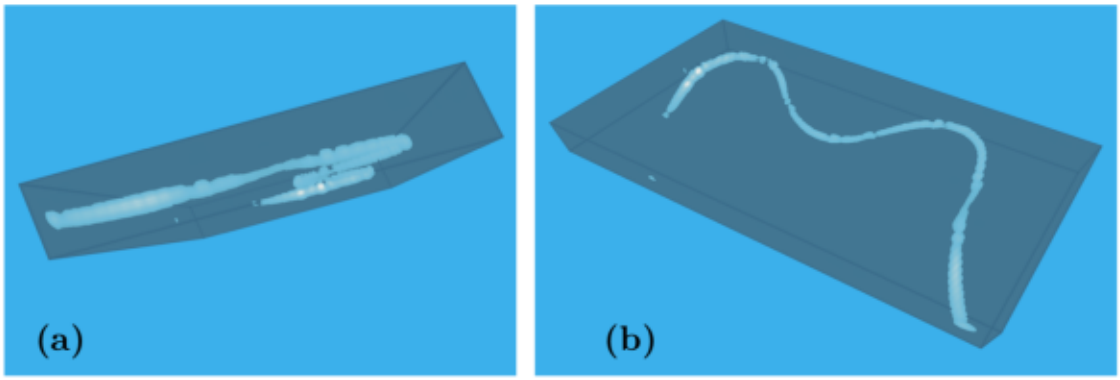

Figure 5. 3D estimated heat sources (i.e., electrical wire) with SVD applied on the measured temperature field number of node of $n_z = 16$ in the z direction and the Fourier number of 0.2 and an L_1 regularization method: view along the thickness (**a**) and along the x and y plane (**b**).

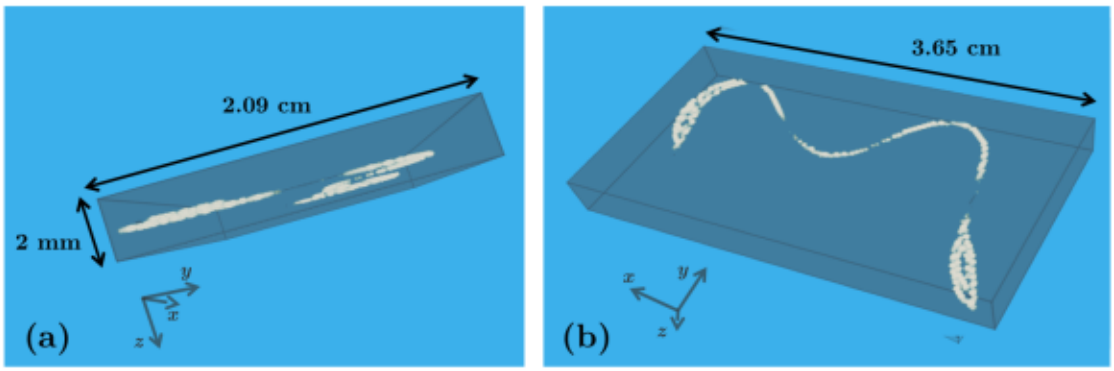

Figure 6. Wire reconstruction using the Bayesian inference method: (**a**) profile view, (**b**) front view.

temperature field, the probabilistic approach reconstruction algorithm is then applied and the solution obtained is illustrated in Figure 6 representing the probability of the presence of source at each point of the plane. The solution given by the program is a 3D matrix, which represents the volume of the sample, where each point of the matrix contains the probability (¿98%) of the presence of a source at this point. The depths of the sources are well found with this method on average; the wire is reconstructed on the plane parallel to the surface, in the center of the plate. Regarding the reconstruction in the x and y directions, the wire is rebuilt thicker than it actually is, especially in areas where the temperature variation is greater. This error is due to the fact that the algorithm considers a constant intensity at any point of the wire. It can also be noted in Figure 6a that in these areas, the wire is reconstructed at a slightly higher position.

Finally, an important point to highlight is the execution time of the program. The calculation in Ref. 28, run on a laptop computer (the least powerful of the computers tested) lasted 8.35 s. To compare, in Ref. 29, the proposed reconstruction method based on SVD and regularization allows estimating the sources for the same experimental problem. Even if a reduction of the study domain is applied, the execution time of the program is particularly long, more than 6 h are necessary to reconstruct the same sources. The Bayesian approach is therefore definitely faster than a deterministic approach.

5. CONCLUSIONS

The subject of this work is to characterize 3D heat sources buried in a material from the temperature field measured at the surface. Measurement noise is an important problem for the reconstruction of heat sources because the problem is mathematically ill-posed. Two different methods has been presented in this paper.

The first method consists in an inverse method based on SVD and regularization that allows estimating the geometry and the intensity of several volumetric sources. The commonly used solution in order to bypass the problem of noise is to add terms of regularization. Two types of regularization were presented in this paper.

Second, a method based on Bayesian approach has been proposed. It constitutes another way to overcome the ill-posed problem of the inversion of a heat equation rather than regularization. The main advantage of this proposed method is the low noise sensitivity and the calculation time compared to other methods.

Both methods was used on an experimental case based on volumic source generated by using a well-controlled Joule effect. It can be noted that the method can be developed to simultaneously estimate the location and the amplitude of the source and a completely non-destructive test can be performed from such methods.

ACKNOWLEDGMENTS

This research was supported by "Projet Région Nouvelle-Aquitaine" and Direction Générale de l'Armement (DGA) funding.

REFERENCES

[1] Crowther, D., Favro, L., Kuo, P., and Thomas, R., "Inverse scattering algorithm applied to infrared thermal wave images," *Journal of applied physics* **74**(9), 5828–5834 (1993).

[2] Mendioroz, A., Castelo, A., Celorrio, R., and Salazar, A., "Characterization of vertical buried defects using lock-in vibrothermography: I. direct problem," *Measurement Science and Technology* **24**(6), 065601 (2013).

[3] Mendioroz, A., Castelo, A., Celorrio, R., and Salazar, A., "Characterization and spatial resolution of cracks using lock-in vibrothermography," *NDT & E International* **66**, 8–15 (2014).

[4] Mendioroz, A., Celorrio, R., Cifuentes, A., Zatón, L., and Salazar, A., "Sizing vertical cracks using burst vibrothermography," *NDT & E International* **84**, 36–46 (2016).

[5] Celorrio, R., Mendioroz, A., and Salazar, A., "Characterization of vertical buried defects using lock-in vibrothermography: Ii. inverse problem," *Measurement Science and Technology* **24**(6), 065602 (2013).

[6] Mendioroz, A., Castelo, A., Celorrio, R., and Salazar, A., "Defect characterization from lock-in vibrothermography data," *International Journal of Thermophysics* **36**(5-6), 1208–1216 (2015).

[7] Burgholzer, P., Thor, M., Gruber, J., and Mayr, G., "Three-dimensional thermographic imaging using a virtual wave concept," *Journal of Applied Physics* **121**(10), 105102 (2017).

[8] Waters, S., Burgholzer, P., Mendioroz, A., and de Ocáriz, I. S., "3d reconstruction of tilted cracks using infrared thermography and the virtual wave concept,"

[9] Özışık, M. N., [*Heat conduction*], John Wiley & Sons (1993).

[10] Maillet, D., [*Thermal quadrupoles: solving the heat equation through integral transforms*], John Wiley & Sons Inc (2000).

[11] Gray, R. M. et al., "Toeplitz and circulant matrices: A review," *Foundations and Trends® in Communications and Information Theory* **2**(3), 155–239 (2006).

[12] Moore, E. H., "On the reciprocal of the general algebraic matrix," *Bull. Am. Math. Soc.* **26**, 394–395 (1920).

[13] Penrose, R., "A generalized inverse for matrices," in [*Mathematical proceedings of the Cambridge philosophical society*], **51**(3), 406–413, Cambridge University Press (1955).

[14] Stewart, G. W., "On the early history of the singular value decomposition," *SIAM review* **35**(4), 551–566 (1993).

[15] Jordan, C., "Sur la réduction des formes bilinéaires," *Comptes Rendus de l'Académie des Sciences* **78**, 614–617 (1874).

[16] Sylvester, J. J., "Sur la reduction biorthogonale d'une forme lineo-linéaire a sa forme canonique," *Comptes Rendus* **108**, 651–653 (1889).

[17] Picard, É., "Sur un theoreme general relatif aux equations integrales de premiere espece et sur quelques problemes de physique mathematique," *Rendiconti del Circolo Matematico di Palermo (1884-1940)* **29**(1), 79–97 (1910).

[18] Hadamard, J., [*Lectures on Cauchy's problem in linear partial differential equations*], vol. 37, Yale University Press (1923).

[19] Vogel, C. R., [*Computational methods for inverse problems*], vol. 23, Siam (2002).

[20] Hanke, M. and Hansen, P. C., "Regularization methods for large-scale problems," *Surv. Math. Ind* **3**(4), 253–315 (1993).

[21] Hansen, P. C., [*Rank-deficient and discrete ill-posed problems: numerical aspects of linear inversion*], vol. 4, Siam (2005).

[22] Hansen, P. C. and O'Leary, D. P., "The use of the l-curve in the regularization of discrete ill-posed problems," *SIAM Journal on Scientific Computing* **14**(6), 1487–1503 (1993).

[23] Thompson, A. M., Brown, J. C., Kay, J. W., and Titterington, D. M., "A study of methods of choosing the smoothing parameter in image restoration by regularization," *IEEE Transactions on Pattern Analysis & Machine Intelligence* (4), 326–339 (1991).

[24] Tikhonov, A. N., "On the solution of ill-posed problems and the method of regularization," in [*Doklady Akademii Nauk*], **151**(3), 501–504, Russian Academy of Sciences (1963).

[25] Tibshirani, R., "Regression shrinkage and selection via the lasso," *Journal of the Royal Statistical Society: Series B (Methodological)* **58**(1), 267–288 (1996).

[26] Bayes, T., "An essay towards solving a problem in the doctrine of chances. 1763.," *MD computing: computers in medical practice* **8**(3), 157 (1991).

[27] Kaipio, J. and Somersalo, E., [*Statistical and computational inverse problems*], vol. 160, 49–112, Springer Science & Business Media (2006).

[28] Groz, M.-M., Abisset-Chavanne, E., Meziane, A., Sommier, A., and Pradère, C., "Bayesian inference for 3d volumetric heat sources reconstruction from surfacic ir imaging," *Applied Sciences* **10**(5), 1607 (2020).

[29] Groz, M.-M., Abisset-Chavanne, E., Meziane, A., Sommier, A., and Pradère, C., "Three-dimensional reconstruction of thermal volumetric sources from surface temperature fields measured by infrared thermography," *Applied Sciences* **9**(24), 5464 (2019).